Dyes and Pigments 95 (2012) 244–251

Contents lists available at SciVerse ScienceDirect

Dyes and Pigments

journal homepage: www.elsevier.com/locate/dyepig

New efficient dyes containing *tert*-butyl in donor for dye-sensitized solar cells

Jie Shi [a], Zhaofei Chai [a], Cheng Zhong [a], Wenjun Wu [b], Jianli Hua [b], Yongqiang Dong [c], Jingui Qin [a], Qianqian Li [a,**], Zhen Li [a,*]

[a] Department of Chemistry, Hubei Key Lab on Organic and Polymeric Opto-Electronic Materials, Wuhan University, Wuhan 430072, China
[b] Key Laboratory for Advanced Materials and Institute of Fine Chemicals, East China University of Science & Technology, Shanghai 200237, China
[c] Department of Chemistry, Beijing Normal University, Beijing 100875, China

ARTICLE INFO

Article history:
Received 15 January 2012
Received in revised form
23 March 2012
Accepted 26 March 2012
Available online 20 April 2012

Keywords:
Tert-butyl
Triphenylamine
Anti-aggregation
Dye-sensitized solar cells
Sensitizers
Power conversion effciency

ABSTRACT

A series of D–π–A organic sensitizers that contains two 4-*tert*-butylbenzene moieties in the donor part of triphenylamine group are designed and characterized. All these dyes comprise the same donor and acceptor units while the different aromatic units are introduced as linkers between the donor and acceptor units. It is found that the tuning of the HOMO and LUMO energy level can be conveniently achieved by alternating the conjugate bridge. The DSSCs based on **LI-17** show the best light to electricity conversion efficiency of 5.35% (J_{sc} = 12.65 mA cm^{-2}, V_{oc} = 675 mV, *ff* = 0.63) under standard global AM 1.5 solar light conditions (100 mW cm^{-2}), indicating that the introduction of *tert*-butyl groups may be able to play an anti-aggregation effect.

1. Introduction

With the consumption of fossil energy and the increasing intensity of global warming, solar energy will play an important role in the future world for its feature of renewable and clean [1]. In 1991, dye-sensitized solar cells (DSSCs) was first fabricated with the Ru-complexes dye, and now some Ru sensitizers could achieve the power conversion efficiencies in excess of 11% subsequently [2–11]. However, due to its rarity of this precious metal, large amounts of researches have been carried out on metal-free organic dyes for its advantages of low cost, easy synthesis, and high molar coefficient. In order to improve photovoltaic efficiencies of DSSCs, many metal-free dyes have been synthesized and shown impressive η values in the range of 5–10.3% [12–32]. Four critical processes determine the photovoltaic performance of the DSSCs: electron injection from the dye to the conduction band of TiO_2; recombination of the injected electrons on TiO_2 with the oxidized dye; dark current generated due to the reduction of I_3^- by the injected electrons; and the regeneration of the dye by the electrolyte which is dependent on the HOMO level of the dye and the redox potential of the electrolyte [33–36]. From the viewpoint of chemists, it is necessary to remodel the molecular design of dyes. And an effective method to improve photovoltaic performance of DSSCs is to inhibit intermolecular π–π aggregation. The phenomenon of π-stacked aggregation on the TiO_2 electrodes always shortens the lifetime of excited electrons which results in decreased photocurrent or leads to molecules residing in the system that are not functionally attached to the surface of TiO_2 and thus act as filters, directly decreasing the electron injection greatly [37,38]. To weaken or avoid the aggregation from a strong intermolecular π–π interaction, some co-adsorbents such as deoxycholic acid (DCA) or chenodeoxycholic acid (CDCA) have often been utilized with the aim to enhance its performance in devices [39,40]. In addition, possible aggregation could be avoided through appropriate structural modification such as introducing alkyl to aniline and thiophene units [41–46]. Aromatic rings have also been introduced to pyrrole *via* N–H bond in order to restrain the aggregation of the dyes and achieve good performance in our previous research [47–49]. Thiophene derivatives have been widely used as conjugated bridge for sensitizers because of their high polarizability, tunable spectroscopic and electrochemical properties. A lot of studies are concerning dyes containing thiophene or furan as conjugated bridge, which reached high photovoltaic efficiencies. However, it is relatively difficult to introduce anti-

* Corresponding author. Tel.: +86 27 62254108; fax: +86 27 68756757.
** Corresponding author. Tel.: +86 27 62306885; fax: +86 27 68756757.
E-mail addresses: qianqian-alinda@163.com (Q. Li), lizhen@whu.edu.cn (Z. Li).

0143-7208/$ – see front matter © 2012 Elsevier Ltd. All rights reserved.
doi:10.1016/j.dyepig.2012.03.027

aggregation group to thiophene and furan units [50–53]. Therefore, we try to synthesize the molecules which contain anti-aggregation groups in donor, and set thiophene derivatives and furan as conjugated bridge.

Tert-butyl was widely used in many opto-electronic materials such as organic light-emitting diodes (OLED), for its superior performance in preventing π–π stacking. Some dyes possess coplanar structure also introduced *tert*-butyl to inhibit aggregation [54–56]. Interestingly, a few research groups reported some D–π–A dyes bearing *tert*-butyl moiety and its functions in molecule design was to improve the solubility [57]. Herein, two 4-*tert*-butylbenzene moieties were chosen as additional groups of triphenylamine. First, the solubility of the dye will be significantly improved; secondly, the introduction of the benzene ring could expand the molecular conjugated system thus enhancing their ability of light harvesting, and thirdly, there are two *tert*-butyl in the donor side just like two umbrellas, which keep a certain distance between molecules, reflecting their function to prevent aggregation. Thiophene, 2,2′-bithiophene, 3,4-ethylenedioxythiophene (EDOT) and furan group were selected to serve as conjugation bridge for their excellent performance in electronic transmission (Scheme 1).

2. Experimental

2.1. Materials

Tetrahydrofuran (THF) was dried over and distilled from K–Na alloy under an atmosphere of dry nitrogen. *N,N*-Dimethylformamide (DMF) was dried over and distilled from CaH_2 under an atmosphere of dry nitrogen. 1,2-Dichloromethane was dried over and distilled from phosphorus pentoxide. Phosphorus oxychloride was freshly distilled before use. All reagents were purchased from Alfa Aesar and used as received. Compound 2- and 4-(diphenylamino)benzaldehyde was prepared following the procedure reported in the literature [58].

2.2. Instrumentation

^1H and ^{13}C NMR spectroscopy study was conducted with a Varian Mercury 300 spectrometer using tetramethylsilane (TMS; $\delta = 0$ ppm) as internal standard. UV–visible spectra were obtained using a Shimadzu UV-2550 spectrometer. Differential pulse voltammetric (DPV) was carried out on a CHI 660 voltammetric analyzer at room temperature in nitrogen-purged anhydrous acetonitrile with tetrabutylammonium hexafluorophosphate ($TBAPF_6$) as the supporting electrolyte at a scanning rate of 100 mV/s. A platinum disk and an Ag/AgCl electrode were used as the working electrode and quasi-reference electrode, respectively. The ferrocene/ferrocenium redox couple was used for potential calibration. Elemental analyses were performed by a Carlo Erba 1106 microelemental analyzer. HR-ESI-TOF mass spectra were recorded on a Waters Micromass LCT Premier XE.

2.2.1. Synthesis of 4-(bis-(4-bromo-phenyl)-amino)-benzaldehyde

To a solution of 4-(diphenylamino) benzaldehyde (30 mmol, 8.0 g) in dichloromethane (150 mL) was added bromine (60.0 mmol, 9.6 g) dropwise within 1.5 h at 0 °C. The resultant mixture was stirred at room temperature for 6 h and then aqueous KOH was added. The mixture was extracted with dichloromethane. The organic layer was collected, washed with water, dried over anhydrous sodium sulfate. Filtered and the solvent was removed by rotator evaporation. The residue was purified by column chromatography over silica gel to give the product (9.20 g, 71%) as green yellow solid. ^1H NMR ($CDCl_3$, 300 MHz) δ (ppm): 9.84 (s, 1H, –CHO), 7.71 (d, $J = 8.7$ Hz, 2H, ArH), 7.48 (d, $J = 8.7$ Hz, 4H, ArH), 7.06–7.01 (m, 6H, ArH).

2.2.2. Synthesis of **1**

A mixture of 4-(bis-(4-bromo-phenyl)-amino)-benzaldehyde (11.6 mmol, 5.0 g), 4-*tert*-butylphenylboronic acid (25.5 mmol, 4.5 g), sodium carbonate (10.0 or 20.0 equiv), THF (monomer concentration about 0.025 M)/water (2:1 in volume), and tetrakis(triphenylphosphine)palladium $Pd(PPh_3)_4$ (3–5 mol%) was carefully degassed and charged with nitrogen. The reaction was stirred for 32 h at 80 °C. After cooled to room temperature, the organic layer was separated, dried over sodium sulfate, and evaporated to dryness. The crude product was purified by column chromatography over silica gel to give the product (4.84 g, 78%) as a yellow solid. Yield: 75%. ^1H NMR ($CDCl_3$, 300 MHz) δ (ppm): 9.76 (s, 1H, –CHO), 7.64 (d, $J = 8.1$ Hz, 1H, ArH), 7.55–7.41 (m, 8H, ArH), 7.26–7.16 (m, 5H, ArH), 7.06 (d, $J = 4.8$ Hz, 2H, ArH), 6.98 (d, $J = 8.1$ Hz, 2H, ArH), 6.91–6.83 (m, 2H, ArH), 1.36 (s, 18H, $-CH_3$).

2.2.3. General synthesis of ***3a–d***

To a solution of the (4-(bis(4′-tert-butylbiphenyl-4-yl)amino) phenyl)methanol (5.4 g, 10 mmol) in 25 mL triethylphosphite was added iodine (2.53 g, 10 mmol) at 0 °C slowly. The resulting mixture was stirred for 5 min at 0 °C, then warmed to room temperature and stirred for 2.5 h. After evaporation of triethylphosphite, column chromatography and removal of trace triethyl phosphate under vacuum at 50 °C afforded compound **2** as light green solid (5.33 g, 85%). Compound **2** (3 mmol) was suspended in 20 mL of anhydrous

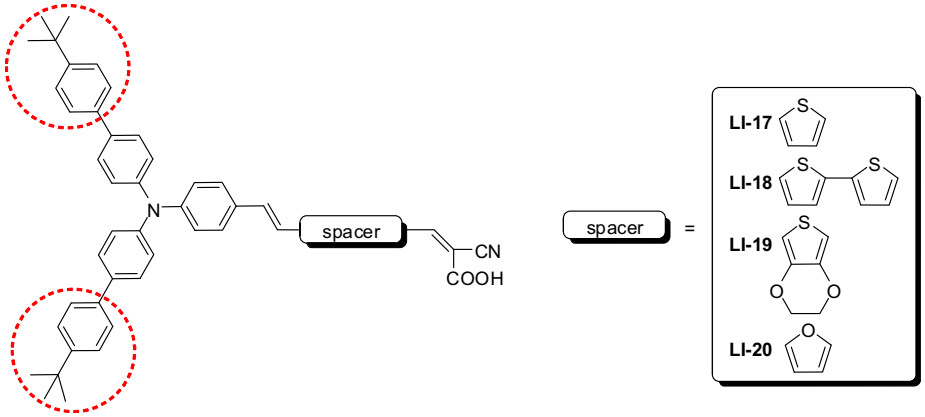

Scheme 1. The structures of **LI-17**, **LI-18**, **LI-19** and **LI-20**.

tetrahydrofuran under an atmosphere of dry nitrogen. *t*-BuOK (0.56 g, 5 mmol) was added directly as a solid and the resultant mixture was stirred at room temperature for 10 min. After the addition of the solution of thiophene-2-carbaldehyde, 2,2′-bithiophene-5-carbaldehyde, 3,4-ethylene-dioxothio-phene-2-carbaldehyde or furan-2-carbaldehyde (2.5 mmol) in anhydrous tetrahydrofuran (20 mL) dropwise, the reaction mixture was stirred at room temperature overnight, then poured into 100 mL of water. The organic product was extracted with chloroform, and dried over anhydrous Na_2SO_4. After removing the solvent, the crude product was purified through a silica gel chromatography column.

2.2.3.1. ***3a***. Light yellow solid. Yield: 74%. ^{1}H NMR ($CDCl_3$, 300 MHz) δ (ppm): 7.52–7.40 (m, 12H, ArH), 7.31 (d, J = 8.1 Hz, 4H, ArH), 7.21–7.09 (m, 7H, ArH), 6.99 (s, 1H, −CH═CH−), 6.77 (s, 1H, −CH═CH−), 1.37 (s, 18H, $-CH_3$). Anal. Calcd for: $C_{44}H_{43}NS$: C, 85.53; H, 7.01; N, 2.27; Found: C, 85.71; H, 6.94; N, 2.15.

2.2.3.2. ***3b***. Pale yellow solid. Yield: 81%. ^{1}H NMR ($CDCl_3$, 300 MHz) δ (ppm): 7.52–7.44 (m, 13H, ArH), 7.37 (d, J = 8.1 Hz, 2H, ArH), 7.21–7.06 (m, 9H, ArH), 6.94 (s, 1H, ArH), 6.85 (d, J = 16 Hz, 2H, −CH═CH−), 1.37 (s, 18H, $-CH_3$). Anal. Calcd for: $C_{48}H_{45}NS_2$: C, 82.36; H, 6.48; N, 2.00; Found: C, 82.63; H, 6.42; N, 2.23.

2.2.3.3. ***3c***. Yellow solid. Yield: 82%. ^{1}H NMR ($CDCl_3$, 300 MHz) δ (ppm): 7.47–7.37 (m, 10H, ArH), 7.28 (d, J = 8.1 Hz, 2H, ArH), 7.11 (d, J = 8.1 Hz, 4H, ArH), 7.05–7.01 (t, J = 14.4 Hz, 3H, ArH), 6.95 (s, 1H, ArH), 6.78 (s, 1H, −CH═CH−), 6.72 (s, 1H, −CH═CH−), 6.13 (s, 1H, ArH), 4.16 (t, J = 21.3 Hz, 4H, $-CH_2-$), 1.29 (s, 18H, $-CH_3$). Anal. Calcd for: $C_{46}H_{45}NO_2S$: C, 81.74; H, 6.71; N, 2.07; Found: C, 81.61; H, 6.63; N, 1.92.

2.2.3.4. ***3d***. Yellow solid. Yield: 65%. ^{1}H NMR ($CDCl_3$, 300 MHz) δ (ppm): 7.50–7.38 (m, 10H, ArH), 7.29 (d, J = 8.1 Hz, 2H, ArH), 7.19 (d, J = 7.5 Hz, 2H, ArH), 7.15–7.04 (m, 9H, ArH), 6.97 (s, 1H, −CH═CH−), 6.81 (s, 1H, −CH═CH−), 1.36 (s, 18H, $-CH_3$). Anal. Calcd for: $C_{44}H_{43}NO$: C, 87.81; H, 7.20; N, 2.33; Found: C, 87.56; H, 6.98; N, 2.51.

2.2.4. General synthesis of ***4a–d***

DMF (2.4 mmol) was added to freshly distilled $POCl_3$ (1.8 mmol) under an atmosphere of dry nitrogen at 0 °C, and the resultant solution was stirred until its complete conversion into a glassy solid. After the addition of compound **3a–d** (1.2 mmol) in 1,2-dichloromethane (20 mL) dropwise, the mixture was stirred at room temperature overnight, then poured into an aqueous solution of sodium acetate (1 M, 300 mL), and stirred for another 2 h. The mixture was extracted with chloroform for several times, the organic fractions were combined and dried over anhydrous Na_2SO_4. After removing the solvent under vacuum, the crude product was purified through a silica gel chromatography column.

2.2.4.1. ***4a***. Red solid. Yield: 80%. ^{1}H NMR ($CDCl_3$, 300 MHz) δ (ppm): 9.85 (s, 1H, −CHO), 7.67 (s, 1H, ArH), 7.53–7.39 (m, 15H, ArH), 7.22–7.11 (m, 8H, ArH, −CH═CH−), 1.37 (s, 18H, $-CH_3$). Anal. Calcd for: $C_{45}H_{45}NOS$: C, 83.68; H, 6.71; N, 2.17; Found: C, 83.79; H, 6.76; N, 2.01.

2.2.4.2. ***4b***. Red solid. Yield: 61%. ^{1}H NMR ($CDCl_3$, 300 MHz) δ (ppm): 9.77 (s, 1H, −CHO), 7.59 (s, 1H, ArH), 7.44–7.37 (m, 12H, ArH), 7.30 (d, J = 7.5 Hz, 2H, ArH), 7.18–7.04 (m, 8H, ArH), 6.98–6.82 (m, 3H, ArH, −CH═CH−), 1.29 (s, 18H, $-CH_3$). $C_{49}H_{45}NOS_2$: C, 80.84; H, 6.23; N, 1.92; Found: C, 80.50; H, 6.54; N, 1.74.

2.2.4.3. ***4c***. Red solid. Yield: 66%. ^{1}H NMR ($CDCl_3$, 300 MHz) δ (ppm): 9.88 (s, 1H, −CHO), 7.51–7.38 (m, 12H, ArH), 7.21–7.01 (m, 8H, ArH), 6.91 (s, 1H, −CH═CH−), 6.80 (s, 1H, −CH═CH−), 4.37 (t, J = 27.3 Hz, 4H, $-CH_2-$), 1.36 (s, 18H, $-CH_3$). $C_{47}H_{45}NO_3S$: C, 80.19; H, 6.44; N, 1.99; Found: C, 80.29; H, 6.49; N, 1.52.

2.2.4.4. ***4d***. Red solid. Yield: 72%. ^{1}H NMR ($CDCl_3$, 300 MHz) δ (ppm): 9.57 (s, 1H, −CHO), 7.52–7.39 (m, 11H, ArH), 7.33 (s, 1H, ArH), 7.22–7.12 (m, 8H, ArH), 6.82 (d, J = 16.5 Hz, 2H, −CH═CH−), 6.49 (s, 2H, ArH), 1.36 (s, 18H, $-CH_3$). $C_{45}H_{43}NO_2$: C, 85.81; H, 6.88; N, 2.22; Found: C, 85.46; H, 6.62; N, 2.08.

2.2.5. General synthesis of ***LI-17–LI-20***

A mixture of **4a–d** (1.00 equiv) and cyanoacetic acid (1.20 equiv) were vacuum-dried, then MeCN (30 mL), THF (30 mL) and piperidine (10 μL) were added. The solution was refluxed for 3–6 h. After the solution was cooled, the organic layer was removed under vacuum. The pure product was purified by recrystallization or column chromatography.

2.2.5.1. LI-17. Dark red solid. Yield: 67%. ^{1}H NMR ($CDCl_3$, 300 MHz) δ (ppm): 8.41 (s, 1H, −CH═), 7.89 (s, 1H, ArH), 7.58–7.38 (m, 15H, ArH), 7.24 (s, 1H, ArH), 7.19 (s, 1H, ArH), 7.09 (d, J = 6.3 Hz, 4H, ArH), 6.97 (d, J = 6.6 Hz, 2H, −CH═CH−), 1.27 (s, 18H, $-CH_3$). ^{13}C NMR (DMSO-d_6, 75 MHz) δ (ppm): 164.4, 150.2, 148.0, 146.2, 137.2, 135.8, 134.6, 132.5, 130.7, 129.1, 128.3, 127.5, 126.6, 126.3, 125.4, 123.2, 117.6, 97.8, 34.8, 31.7. HRMS (HR-ESI-TOF): m/z calcd for $C_{48}H_{44}N_2O_2S$ $[M + H]^+$ 713.3202, found 713.3206.

2.2.5.2. LI-18. Dark red solid. Yield: 71%. ^{1}H NMR ($CDCl_3$, 300 MHz) δ (ppm): 8.42 (s, 1H, −CH═), 7.93 (s, 1H, ArH), 7.59–7.37 (m, 17H, ArH), 7.31 (s, 1H, ArH), 7.20 (s, 1H, ArH), 7.10 (d, J = 7.2 Hz, 4H, ArH), 6.99 (d, J = 8.1 Hz, 2H, −CH═CH−), 1.28 (s, 18H, ArH). ^{13}C NMR (DMSO-d_6, 75 MHz) δ (ppm): 164.3, 150.1, 147.4, 146.4, 145.6, 141.5, 137.2, 135.6, 134.7, 133.8, 131.3, 129.9, 128.5, 128.2, 126.6, 126.3, 125.1, 123.7, 117.6, 99.8, 34.8, 31.7. HRMS (HR-ESI-TOF): m/z calcd for $C_{52}H_{47}N_2O_2S_2$ $[M + H]^+$ 795.3079, found 795.3096.

2.2.5.3. LI-19. Dark red solid. Yield: 65%. ^{1}H NMR ($CDCl_3$, 300 MHz) δ (ppm): 8.16 (s, 1H, −CH═), 7.61–7.44 (m, 10H, ArH), 7.43 (d, J = 8.1 Hz, 4H, ArH), 7.18–7.10 (m, 6H, ArH), 6.96 (d, J = 8.1 Hz, 2H, −CH═CH−), 4.43 (t, J = 24.8 Hz, 4H, $-CH_2-$), 1.29 (s, 18H, $-CH_3$). ^{13}C NMR (DMSO-d_6, 75 MHz) δ (ppm): 163.7, 148.9, 148.2, 146.7, 144.9, 138.0, 135.9, 134.6, 131.2, 130.9, 129.3, 127.7, 127.0, 125.3, 125.1, 124.2, 121.8, 116.7, 92.9, 64.1, 33.6, 30.5. HRMS (HR-ESI-TOF): m/z calcd for $C_{50}H_{47}N_2O_4S$ $[M + H]^+$ 771.3257, found 771.3234.

2.2.5.4. LI-20. Dark red solid. Yield: 80%. ^{1}H NMR ($CDCl_3$, 300 MHz) δ (ppm): 7.99 (s, 1H, −CH═), 7.63–7.42 (m, 14H, ArH), 7.34 (s, 1H, ArH), 7.29 (s, 1H, ArH), 7.13 (d, 2H, ArH), 7.03 (d, 4H, ArH), 6.84 (s, 2H, −CH = CH−), 1.30 (s, 18H, $-CH_3$). ^{13}C NMR (DMSO-d_6, 75 MHz) δ (ppm): 164.9, 159.7, 150.4, 148.4, 146.4, 137.8, 137.4, 136.1, 133.4, 130.6, 129.4, 128.5, 126.8, 126.5, 125.7, 123.5, 117.7, 98.1, 35.1, 31.9. HRMS (HR-ESI-TOF): m/z calcd for $C_{48}H_{44}N_2O_3$ $[M + H]^+$ 697.3430, found 697.3425.

2.3. Device fabrication

A layer of *ca.* 5 μm TiO_2 (13 nm paste, T/SP) was coated on the FTO conducting glass by screen printing and then dried for 6 min at 125 °C. This procedure was repeated 2 times (*ca.* 10 μm) and finally coated by a layer (*ca.* 4 μm) of TiO_2 paste (Ti-nanoxide 300) as the scattering layer. The tri-layer TiO_2 electrodes were gradually heated under an air flow at 275 °C for 5 min, 325 °C for 5 min, 375 °C for 5 min, 450 °C for 15 min, and 500 °C for 15 min. The sintered film was further treated with 0.2 M $TiCl_4$ aqueous solution at room temperature for 12 h, then

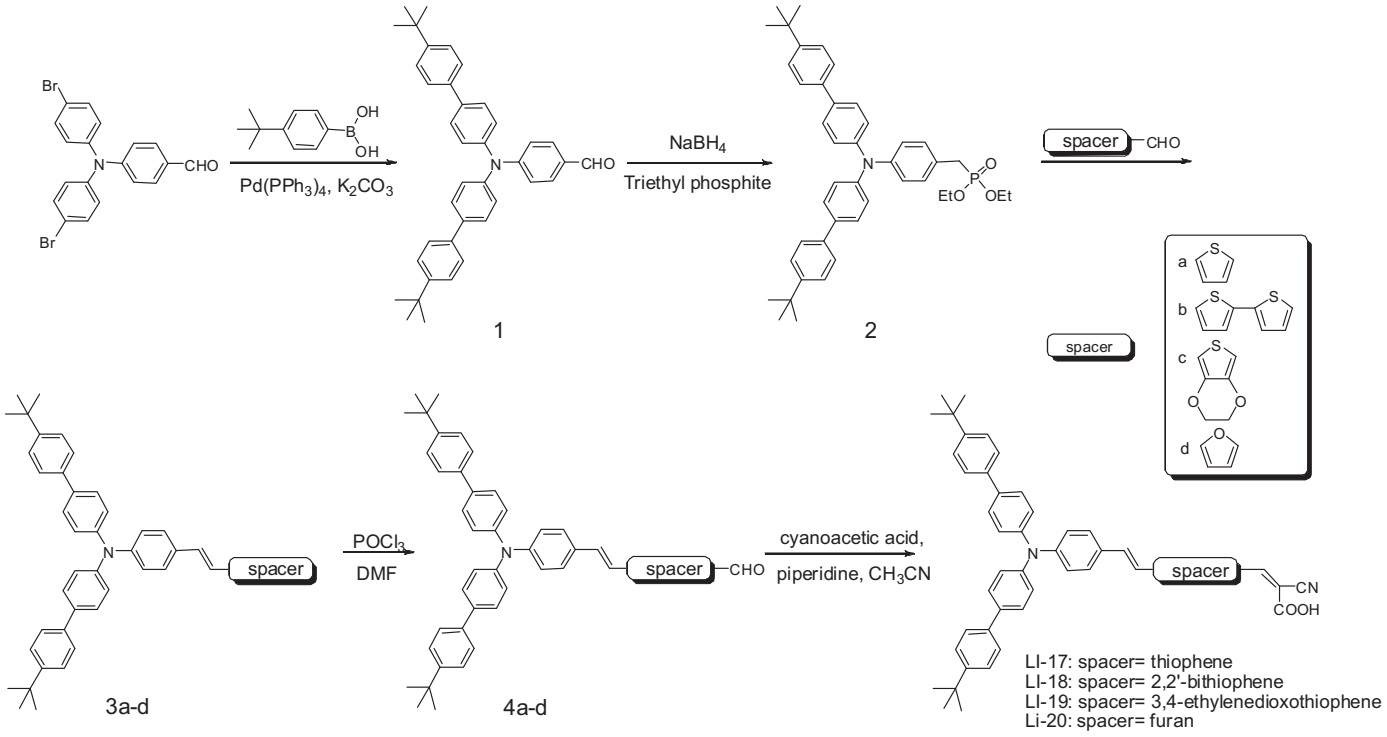

Scheme 2. Synthetic route of **LI-17**, **LI-18**, **LI-19** and **LI-20**.

washed with water and ethanol, and annealed at 450 °C for 30 min. After the film was cooled to 50 °C, it was immersed into a 3×10^{-4} M dye bath in CH_2Cl_2 solution and maintained in the dark for 24 h at room temperature. The electrode was then rinsed with CH_2Cl_2 and dried. The size of the TiO_2 electrodes used was 0.28 cm^2. To prepare the counter electrode, the Pt catalyst was deposited on cleaned FTO glass by coating with a drop of H_2PtCl_6 solution (0.02 M 2-propanol solution) with heat treatment at 400 °C for 15 min. A hole (0.8 mm diameter) was drilled on the counter electrode using a drill-press. The perforated sheet was cleaned with ultrasound in an ethanol bath for 10 min. For the assembly of DSSCs, the dye-covered TiO_2 electrode and Pt-counter electrode were assembled into a sandwich type cell and sealed with a hot-melt gasket of 25 mm thickness made of the ionomer Surlyn 1702 (DuPont). The electrolyte consisting of 0.6 M 1,2-dimethyl-3-propylimidazolium iodide (DMPII), 0.1 M LiI, 0.05 M I_2, and 0.5 M 4-*tert*-butylpyridine (TBP) in a mixture of acetonitrile and methoxypropionitrile (volume ratio, 7:3) was introduced into the cell *via* vacuum backfilling from the hole in the back of the counter electrode. Finally, the hole was sealed using a UV-melt gum and a cover glass.

2.4. Photovoltaic properties measurements

Photovoltaic measurements employed an AM 1.5 solar simulator equipped with a 300 W xenon lamp (Model No. 91160, Oriel). The power of the simulated light was calibrated to 100 mW cm^{-2} using a Newport Oriel PV reference cell system (Model 91150V). *J–V* curves were obtained by applying an external bias to the cell and measuring the generated photocurrent with a Keithley model 2400 digital source meter. The voltage step and delay time of photocurrent were 10 mV and 40 ms, respectively. Cell active area was tested with a mask of 0.196 cm^2. The photocurrent action spectra were measured with an IPCE test system consisting of a Model SR830 DSP Lock-In Amplifier and a Model SR540 Optical Chopper (Stanford Research Corporation, USA), a 7IL/PX150 xenon lamp and power supply, and a 7ISW301 Spectrometer.

3. Results and discussion

3.1. Synthesis of the dyes

The whole synthetic route is shown in Scheme 2. Under the normal Suzuki coupling reaction, **1** was obtained from the bromine atom exposed intermediate and 4-tert-butylphenylboronic acid with good yield. Then, the followed Wittig reaction between **2** and aromatic aldehyde gave the corresponding compounds **3a**–**3d**, which underwent another Vilsmeier reaction to yield the aldehyde **4a**–**4d**. Finally, the four dyes were produced from **4a**–**4d** upon the Knoevenagel condensation reaction with cyanoacetic acid in the presence of piperidine. All the compounds and four new organic sensitizers (**LI-17**–**LI-20**) were confirmed by ^1H and ^{13}C NMR, and HRMS.

3.2. Absorption spectra

The four dyes were soluble in common organic solvents, such as dichloromethane, THF, DMF, and DMSO. As shown in their UV–vis spectra tested in ethanol (Fig. 1, Table 1), two distinct absorptions were observed around 340 and 450 nm. The absorption band around 340 nm was assigned to a $\pi-\pi^*$ transition, while the absorption band with λ_{max} around 450 nm corresponding to an intramolecular charge transfer (ICT) between the TPA donor part and the acceptor end group. The absorption maximum of **LI-20** at 456 nm was red shift by 6 nm in comparison with that of **LI-17**, as **LI-20** containing a furan unit instead of thiophene. And **LI-19**

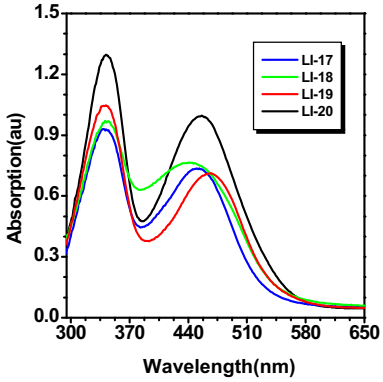

Fig. 1. UV–vis spectra of dyes in ethanol. Concentration: 3.0×10^{-5} mol/L.

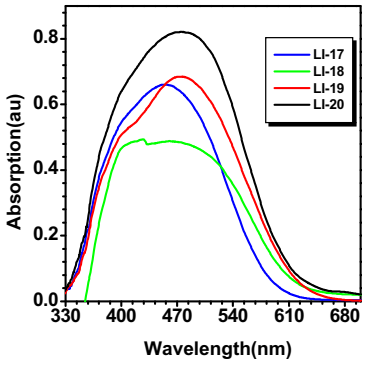

Fig. 2. UV–vis spectra of the dyes on TiO_2 films.

exhibits a red-shift peaks at 467 nm (ε = 37,600 M^{-1} cm^{-1}) in ethanol compared to the others, the appreciable red shift is attributed to the presence of EDOT moieties, which enhanced the extent of electron delocalization over the whole molecule. The molar extinction coefficient of **LI-17**, 24,500 M^{-1} cm^{-1} (450 nm), is much higher than that of **N719**, indicating that these dyes have good light-harvesting ability. Both blue and red shift of the absorption band were reported for dipolar organic dyes upon adsorption on the TiO_2 surface, due to different interaction between the dyes and TiO_2, or between the dyes. In this study, the absorption spectra of the dyes became broadened after adsorption on the TiO_2 surface (Fig. 2), which should favor the light harvesting of the solar cells and thus increase the photocurrent response region, leading to the increase of J_{sc}. The maximum absorption peaks for **LI-17**–**LI-20** on the TiO_2 films are red shift by 4, 27, 6 and 19 nm respectively, in comparison with their spectra in solutions. The red shifts of the absorption spectra on TiO_2 of **LI-17**–**LI-20** are due to the J-aggregation on the TiO_2 surface, in which J-aggregation can also present readily because of the carboxyl unit of the dyes. Such broaden and red-shift absorption has been turned up in other organic dyes, and this phenomenon proves that the introduction of *tert*-butyl may indeed inhibit the $\pi-\pi$ stacking and H-aggregation.

3.3. Electrochemical properties

The oxidation potential of the two dyes was determined from the peak potentials (E_p) by DPV (Fig. 3). The oxidation potential of the dyes was calculated from the peak potentials (E_p) by DPV; the oxidation potential *vs* NHE (E_{ox}) corresponded to the highest occupied molecular orbital (HOMO), while the reduction potential *vs* NHE (E_{red}), which corresponded to the lowest unoccupied molecular orbital (LUMO), could be calculated from E_{ox} to E_{0-0}. Table 1 summarized the electrochemical properties of the four dyes. The potential energy of ionization decreased slightly in the order of **LI-17** > **LI-20** > **LI-19** > **LI-18**. As shown in Fig. 4, the HOMO levels thus obtained within the range of 0.94–1.01 eV, which were more positive than the iodine/iodide redox potential value (0.4 eV), indicating that the oxidized dyes formed after electron injection into the conduction band of TiO_2 could thermodynamically accept electrons from I^- ions. The LUMO levels of the dyes were estimated by the values of E_{ox} and the E_{0-0} band gaps, and these were sufficiently more negative than the conduction-band-edge energy level (E_{cb}) of the TiO_2 electrode (−0.5 V vs. NHE), which implies that electron injection from the excited dye into the conduction band of TiO_2 is energetically permitted.

Table 1
Absorbance and electrochemical properties of dyes.

Dye	λ_{max}[a] (nm)	ε[a] (M^{-1} cm^{-1})	λ_{max}[b] (nm)	E_{0-0}[c] (eV)	E_p[d] (V)	E_{ox}[e] (V) vs NHE	E_{red}[f] (V) vs NHE
LI-17	450	24,500	454	2.29	0.81, 0.93	1.01	−1.28
LI-18	441	32,400	468	2.21	0.74, 0.95	0.94	−1.27
LI-19	467	23,700	473	2.20	0.79	0.99	−1.21
LI-20	456	33,200	475	2.19	0.80	1.00	−1.19

[a] Absorption spectra of dyes measured in ethanol with the concentration of 3×10^{-5} mol/L.
[b] Absorption spectra of dyes adsorbed on the surface of TiO_2.
[c] The band gap, E_{0-0} was derived from the observed optical edge.
[d] E_p is the peak of DPV (the DPV of the dyes were measured in CH_2Cl_2 with 0.1 M $(n\text{-}C_4H_9)_4NPF_6$ as electrolyte (scanning rate, 100 mV/s; working electrode and counter electrode, Pt wires; reference electrode, Ag/AgCl)).
[e] The oxidation potential (E_{ox}) referenced to calibrated Ag/AgCl was converted to the NHE reference scale: $E_{ox} = E_p + 0.197$ V.
[f] E_{red} was calculated from E_{ox} to E_{0-0}.

3.4. Theoretical approach

The structures of the dyes were analyzed using a the B3LYP exchange-correlation functional and a 6-31g* basis set; salvation effects were included by means of the polarizable continuum model to gain further insight into the correlation between structure and the physical properties as well as the device performance. To model the electronic state of the dyes adsorbed on the TiO_2 surface, we employed the carboxylate of the dyes because they should be bonded to the TiO_2 surface in these form. The electron distribution of the HOMO and LUMO of **LI-17**–**LI-20** was shown in Fig. 5. The

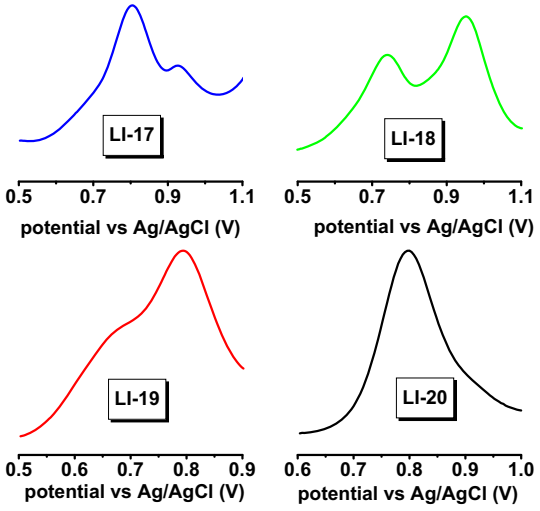

Fig. 3. DPV of dyes.

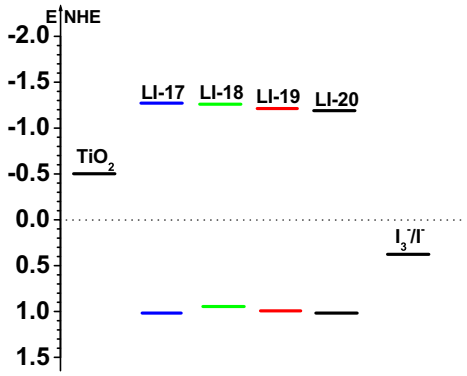

Fig. 4. Schematic representation of the band positions in DSSCs based on **LI-17**–**LI-20**. The energy scale is indicated in electron volts using the normal hydrogen electrode (NHE).

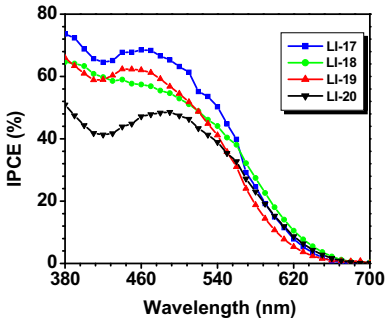

Fig. 6. Spectra of monochromatic incident photon-to-current conversion efficiency (IPCE) for DSSCs based on **LI-17**–**LI-20**.

HOMO consists of delocalized π orbitals on spacer unit, with greatest density in TPA, and the LUMO of dyes show a greater contribution localized in cyanoacrylic acid part, giving the strongest D–A strength. Thus, the HOMO to LUMO excitation induced by light irradiation could move the electron distribution from the whole molecules to the anchoring moieties. As depicted above, it also revealed that the dyes were completely planar except for the 4-*tert*-butylbenzene moieties linked to TPA group to avoid steric clashes, and those bonded on the TPA ring had some electron transition to the planar system. The two *tert*-butyl moieties at the head of the molecule act just like two umbrellas, to keep a certain distance between the dyes when absorbed on TiO_2.

3.5. Photovoltaic performance of DSSCs

The incident photon-to-current conversion efficiencies (IPCEs) of dyes as shown in Fig. 6, were obtained with a sandwich cell using 0.6 M 1-butyl-3-methylimidazolium iodide (BMII), 0.1 M LiI, 0.05 M I_2 and 0.5 M 4-*tert*-butylpyridine (TBP) in dry acetonitrile (CH_3CN). The IPCE of the dyes illustrate that the visible light can be converted to photocurrent efficiently in the region from 400 to 620 nm, and the values were all higher than 50% in the region of 380–510 except **LI-20**. The value of **LI-17** exceeds 60% over the spectral region from 400 to 530 nm, reaching its maximum of 68% at 460 nm. The IPCE values of **LI-18** reached its maximum of 58% at 450 nm. And the **LI-19** reached 62% at 450 nm. From the IPCE performance of dyes, we can infer that, the DSSCs based on **LI-17** would generate the highest conversion yield in these dyes.

Fig. 7 shows the photocurrent–voltage (J–V) plots of DSSCs fabricated with these dyes under AM 1.5G simulated sunlight at 100 mW cm^{-2}, and the pertinent performance data are described in Table 2, the photovoltaic characteristic parameters, i.e., short circuit current (J_{sc}), open-circuit photovoltage (V_{oc}), fill factor (ff), and solar-to-electrical photocurrent density (η). The broadening of the IPCE spectra is desired for a larger photocurrent which explains the higher efficiency observed for the dyes. DSSC based on **LI-17** show the highest solar to electricity conversion efficiency of 5.35% (J_{sc} = 12.65 mA cm^{-2}, V_{oc} = 675 mV, ff = 0.63) among these dyes, which should be ascribed to its best performance in IPCE. From Fig. 4, we observed that the **LI-17** showed the deepest HOMO and broadest band gap, but not the highest V_{oc}, these may ascribe to the charge recombination. The excited state oxidation potentials of the dyes assume the following order: **LI-20** > **LI-19** > **LI-18** > **LI-17**. More negative excited state oxidation potential observed for **LI-17**

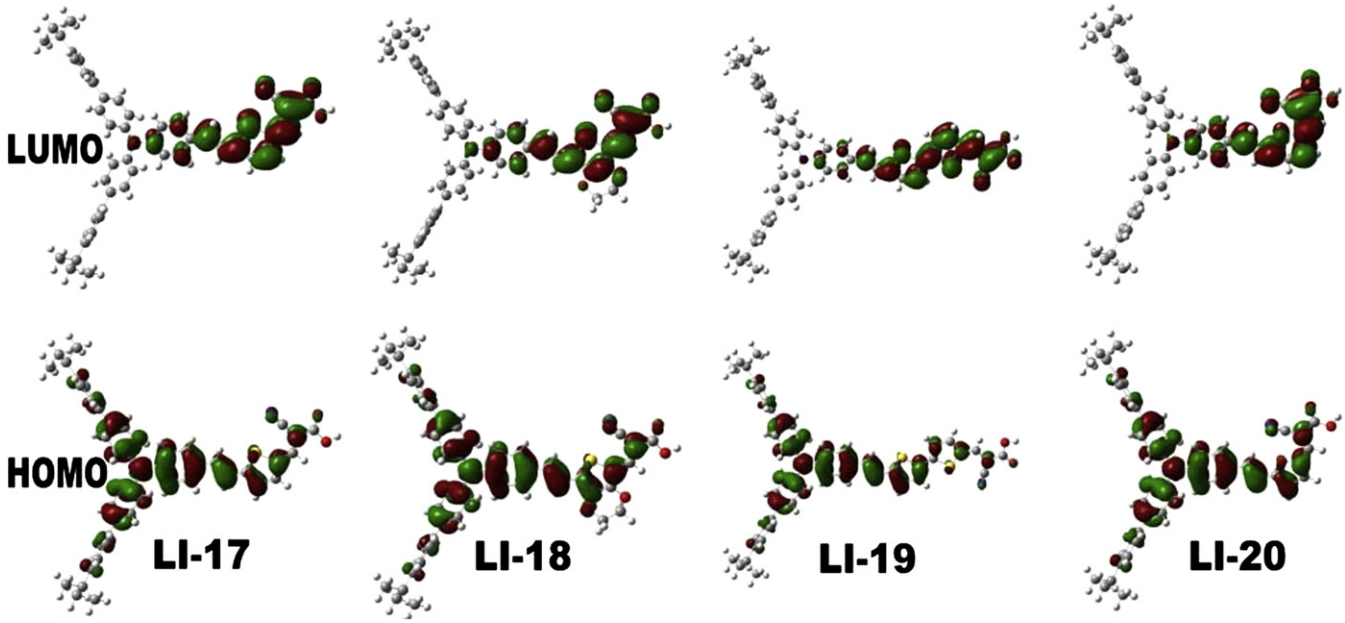

Fig. 5. Frontier orbitals of the dyes **LI-17**–**LI-20** optimized at the B3LYP/6-31+G (D) level.

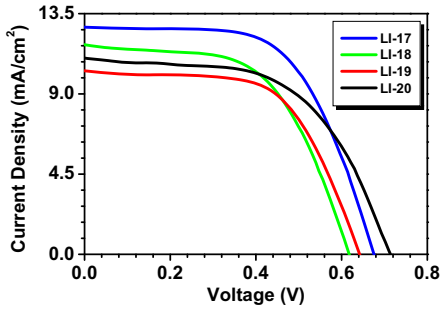

Fig. 7. Current density–voltage characteristics obtained with a nanocrystalline TiO_2 film supported on FTO conducting glass and derivatized with monolayer of the sensitizers.

Table 2
DSSCs performance data of novel dyes[a].

Dye	J_{sc} (mA cm^{-2})	V_{oc} (V)	*ff*	η (%)
LI-17	12.65	0.675	0.63	5.35
LI-18	11.8	0.615	0.58	4.23
LI-19	10.31	0.64	0.62	4.08
LI-20	10.98	0.72	0.57	4.48

[a] Illumination: 100 mW cm^{-2} simulated AM 1.5 G solar light; electrolyte containing: 0.1 M LiI + 0.05 M I_2 + 0.6 M DMPII + 0.5 M TBP in the mixed solvent of acetonitrile and 3-methoxypropionitrile (7:3, v/v).

among the series, gives larger driving force the electron injection from this dye. However, this trend is not matching with the photovoltaic efficiency trend, indicating that other factors also influence the photovoltaic performance. Therefore we believe that the *tert*-butyl in donor does have play an important role in anti-aggregation, but for different structures of the dyes, the effect of the anti-aggregation to the dyes was not similar, and the results indicated that the function is effective to the dyes with thiophene and furan unit but weak to the other units.

4. Conclusions

In conclusion, a new series of organic dyes (**LI-17**–**LI-20**), which contain TPA substituted by two 4-*tert*-butylbenzene moieties as the donor, a cyanoacrylic acid as the acceptor and anchoring groups, and thiophene, 2,2′-bithiophene, 3,4-ethylenedio-xythiophene (EDOT) and furan group as the conjugate bridge, were synthesized and applied in DSSCs. The 4-*tert*-butylbenzene moieties were employed as a part of anti-aggregation group. The absorption spectra, electrochemical and photovoltaic performance of the dyes were studied. Among these dyes, DSSCs based on **LI-17** show the best light to electricity conversion efficiency of 5.35% (J_{sc} = 12.65 mA cm^{-2}, V_{oc} = 675 mV, *ff* = 0.63). The preliminary results demonstrated that the introduction of *tert*-butyl groups may be able to play the anti-aggregation effect, and more follow-up work is being carried out in our laboratory.

Acknowledgments

We are grateful to the National Science Foundation of China (no. 21002075), and the National Fundamental Key Research Program (no. 2011CB932702) for financial support.

References

[1] Armaroli N, Balzani V. The future of energy supply: challenges and opportunities. Angew Chem Int Ed 2007;46:52–66.
[2] O'Regan B, Grätzel M. Low-cost high-efficiency solar cell based on dye-sensitized colloidal TiO_2 films. Nature 1991;353:737–40.
[3] Hagfeldt A, Grätzel M. Molecular photovoltaics. Acc Chem Res 2000;33:269–77.
[4] Grätzel M. Recent advances in sensitized mesoscopic solar cells. Acc Chem Res 2009;42:1788–98.
[5] Yum JH, Walter P, Huber S, Rentsch D, Geiger T, Nüesch F, et al. Efficient far red sensitization of nanocrystalline TiO_2 films by an unsymmetrical squaraine dye. J Am Chem Soc 2007;129:10320–1.
[6] Ito S, Zakeeruddin SM, Humphry-Baker R, Liska P, Charvet R, Comte RP, et al. High efficiency organic dye sensitized solar cells controlled by nanocrystalline-TiO_2 electrode thickness. Adv Mater 2006;18:1202–5.
[7] Hagfeldt A, Grätzel M. Light-induced redox reactions in nanocrystalline systems. Chem Rev 1995;95:49–68.
[8] Grätzel M. Dye-sensitized solar cells. J Photochem Photobiol C 2003;4:145–53.
[9] Nazeeruddin MK, Kay A, Rodicio I, Humphry-Baker R, Müller E, Liska P, et al. Conversion of light to electricity by *cis*-X_2bis(2,2′-bipyridyl-4,4′-dicarboxylate) ruthenium(II) charge-transfer sensitizers (X = Cl–, Br–, I–, CN–, and SCN–) on nanocrystalline titanium dioxide electrodes. J Am Chem Soc 1993;115:6382–90.
[10] Gao F, Wang Y, Shi D, Zhang J, Wang M, Jing X, et al. Enhance the optical absorptivity of nanocrystalline TiO_2 film with high molar extinction coefficient ruthenium sensitizers for high performance dye-sensitized solar cells. J Am Chem Soc 2008;130:10720–8.
[11] Gao F, Wang Y, Zhang J, Shi D, Wang M, Humphy-Baker R, et al. A new heteroleptic ruthenium sensitizer enhances the absorptivity of mesoporous titania film for a high efficiency dye-sensitized solar cell. Chem Commun; 2008:2635–7.
[12] Hara K, Kurashige M, Dan-oh Y, Kasada C, Shinpo A, Suga S, et al. Design of new coumarin dyes having thiophene moieties for highly efficient organic-dye-sensitized solar cells. New J Chem 2003;27:783–5.
[13] Hara K, Sayama K, Ohga Y, Shinpo A, Suga S, Arakawa H. A coumarin-derivative dye sensitized nanocrystalline TiO_2 solar cell having a high solar-energy conversion efficiency up to 5.6%. Chem Commun; 2001:569–70.
[14] Wang ZS, Cui Y, Hara K, Dan-oh Y, Kasada C, Shinpo A. A high-light-harvesting-efficiency coumarin dye for stable dye-sensitized solar cells. Adv Mater 2007;19:1138–41.
[15] Horiuchi T, Miura H, Sumioka K, Uchida S. High efficiency of dye-sensitized solar cells based on metal-free indoline dyes. J Am Chem Soc 2004;126:12218–9.
[16] Horiuchi T, Miura H, Uchida S. Highly-efficient metal-free organic dyes for dye-sensitized solar cells. Chem Commun; 2003:3036–7.
[17] Hara K, Kurashige M, Ito S, Shinpo A, Suga S, Sayama K, et al. Novel polyene dyes for highly efficient dye-sensitized solar cells. Chem Commun; 2003:252–3.
[18] Kitamura T, Ikeda M, Shigaki K, Inoue T, Anderson NA, Ai X, et al. Phenyl-conjugated oligoene sensitizers for TiO_2 solar cells. Chem Mater 2004;16:1806–12.
[19] Hara K, Sato T, Katoh R, Furube A, Yoshihara T, Murai M, et al. Adv Funct Mater 2005;15:246–52.
[20] Liu B, Zhu W, Zhang Q, Wu W, Xu M, Ning Z, et al. Conveniently synthesized isophorone dyes for high efficiency dye-sensitized solar cells: tuning photovoltaic performance by structural modification of donor group in donor-π-acceptor system. Chem Commun; 2009:1766–8.
[21] Sayama K, Tsukagoshi S, Hara K, Ohga Y, Shinpou A, Abe Y, et al. Photoelectrochemical properties of J aggregates of benzothiazole merocyanine dyes on a nanostructured TiO_2 film. J Phys Chem B 2002;106:1363–71.
[22] Sayama K, Hara K, Mori N, Satsuki M, Suga S, Tsukagoshi S, et al. Photosensitization of a porous TiO_2 electrode with merocyanine dyes containing a carboxyl group and a long alkyl chain. Chem Commun; 2000:1173–4.
[23] Yao QH, Shan L, Li FY, Yin DD, Huang CH. An expanded conjugation photosensitizer with two different adsorbing groups for solar cells. New J Chem 2003;27:1277–83.
[24] Chen YS, Li C, Zeng ZH, Wang WB, Wang XS, Zhang BW. Efficient electron injection due to a special adsorbing group's combination of carboxyl and hydroxyl: dye-sensitized solar cells based on new hemicyanine dyes. J Mater Chem 2005;15:1654–61.
[25] Imahori H, Umeyama T, Ito S. Large π-aromatic molecules as potential sensitizers for highly efficient dye-sensitized solar cells. Acc Chem Res 2009;42:1809–18.
[26] Zhou G, Pschirer N, Schoeneboom JC, Eickemeyer F, Baumgarten M, Müellen K. Ladder-type pentaphenylene dyes for dye-sensitized solar cells. Chem Mater 2008;20:1808–15.
[27] Heredia D, Natera J, Gervaldo M, Otero L, Fungo F, Lin CY, et al. Spirobifluorene-bridged donor/acceptor dye for organic dye-sensitized solar cells. Org Lett 2010;12:12–5.
[28] Zeng WD, Cao YM, Bai Y, Wang YH, Shi YS, Zhang M, et al. Efficient dye-sensitized solar cells with an organic photosensitizer featuring orderly conjugated ethylenedioxythiophene and dithienosilole blocks. Chem Mater 2010;22:1915–25.
[29] Wu WJ, Xu XD, Yang HB, Hua JL, Zhang XY, Zhang L, et al. D-π-M-π-A structured platinum acetylide sensitizer for dye-sensitized solar cells. J Mater Chem 2011;21:10666–71.
[30] He XJ, Wu WJ, Hua JL, Jiang YH, Qu SY, Li J, et al. Bithiazole-bridged dyes for dye-sensitized solar cells with high open circuit voltage performance. J Mater Chem 2011;21:6054–62.

[31] Chen BS, Chen DY, Chen CL, Hsu CW, Hsu HC, Wu KL, et al. Donor–acceptor dyes with fluorine substituted phenylene spacer for dye-sensitized solar cells. J Mater Chem 2011;21:1937–45.
[32] Chang YJ, Chow TJ. Highly efficient triarylene conjugated dyes for sensitized solar cells. J Mater Chem 2011;21:9523–31.
[33] Ning ZJ, Tian H. Triarylamine: a promising core unit for efficient photovoltaic materials. Chem Commun; 2009:5483–95.
[34] Hagfeldt A, Boschloo G, Sun LC, Kloo L, Pettersson H. Dye-sensitized solar cells. Chem Rev 2010;110:6595–663.
[35] Ning ZJ, Fu Y, Tian H. Improvement of dye-sensitized solar cells: what we know and what we need to know. Energy Environ Sci 2010;3:1170–81.
[36] Listorti A, O'Regan B, Durrant JR. Electron transfer dynamics in dye-sensitized solar cells. Chem Mater 2011;23:3381–99.
[37] Ito S, Miura H, Uchida S, Takata M, Sumioka K, Liska P, et al. High-conversion-efficiency organic dye-sensitized solar cells with a novel indoline dye. Chem Commun; 2008:5194–6.
[38] Mann JR, Gannon MK, Fitzgibbons TC, Detty MR, Watson DF. Optimizing the photocurrent efficiency of dye-sensitized solar cells through the controlled aggregation of chalcogenoxanthylium dyes on nanocrystalline titania films. J Phys Chem C 2008;112:13057–61.
[39] Tang J, Hua JL, Wu WJ, Li J, Jin ZG, Long YT, et al. New starburst sensitizer with carbazole antennas for efficient and stable dye-sensitized solar cells. Energy Environ Sci 2010;3:1736–45.
[40] Li WQ, Wu YZ, Li X, Xie YS, Zhu WH. Absorption and photovoltaic properties of organic solar cell sensitizers containing fluorene unit as conjunction bridge. Energy Environ Sci 2011;4:1830–7.
[41] Kim S, Lee JK, Kang SO, Ko J, Yum JH, Fantacci S, et al. Molecular engineering of organic sensitizers for solar cell applications. J Am Chem Soc 2006;128:16701–7.
[42] Jung I, Lee JK, Song KH, Song K, Kang SO, Ko J. Synthesis and photovoltaic properties of efficient organic dyes containing the benzo[b]furan moiety for solar cells. J Org Chem 2007;72:3652–8.
[43] Kim S, Kim D, Choi H, Kang MS, Song K, Kang SO, et al. Enhanced photovoltaic performance and long-term stability of quasi-solid-state dye-sensitized solar cells via molecular engineering. Chem Commun; 2008:4951–3.
[44] Hagberg DP, Jiang X, Gabrielsson E, Linder M, Marinado T, Brinck T, et al. Symmetric and unsymmetric donor functionalization. Comparing structural and spectral benefits of chromophores for dye-sensitized solar cells. J Mater Chem 2009;19:7232–8.
[45] Shen P, Liu Y, Huang X, Zhao B, Xiang N, Fei J, et al. Efficient triphenylamine dyes for solar cells: effects of alkyl-substituents and π-conjugated thiophene unit. Dyes Pigm 2009;83:187–97.
[46] Chen H, Huang H, Huang X, Clifford JN, Forneli A, Palomares E, et al. High molar extinction coefficient branchlike organic dyes containing di(p-tolyl) phenylamine donor for dye-sensitized solar cells applications. J Phys Chem C 2010;114:3280–6.
[47] Koumura N, Wang ZS, Mori S, Miyashita M, Suzuki E, Hara K. Alkyl-functionalized organic dyes for efficient molecular photovoltaics. J Am Chem Soc 2006;128:14256–7.
[48] Li Q, Lu L, Zhong C, Huang J, Huang Q, Shi J, et al. New pyrrole-based organic dyes for dye-sensitized solar cells: convenient syntheses and high efficiency. Chem Eur J 2009;15:9664–8.
[49] Li Q, Lu L, Zhong C, Huang Q, Shi J, Jin X, et al. New indole-based metal-free organic dyes for dye-sensitized solar cells. J Phys Chem B 2009;113:14588–95.
[50] Lin JT, Chen PC, Yen YS, Hsu YC, Chou HH, Yeh MCP. Organic dyes containing furan moiety for high-performance dye-sensitized solar cells. Org Lett 2009;11:97–100.
[51] Hagberg DP, Edvinsson T, Marinado T, Boschloo G, Hagfeldt A, Sun LC. A novel organic chromophore for dye-sensitized nanostructured solar cells. Chem Commun; 2006:2245–7.
[52] Li R, Lv X, Shi D, Zhou DF, Cheng YM, Zhang GL, et al. Dye-sensitized solar cells based on organic sensitizers with different conjugated linkers: furan, bifuran, thiophene, tithiophene, selenophene, and biselenophene. J Phys Chem C 2009;113:7469–79.
[53] Heo JY, Oh JW, Ahn HI, Lee SB, Choc SE, Kim MR, et al. Synthesis and characterization of triphenylamine-based organic dyes for dye-sensitized solar cells. Synth Met 2010;160:2143–50.
[54] Mathew S, Imahori H. Tunable, strongly-donating perylene photosensitizers for dye-sensitized solar cells. J Mater Chem 2011;21:7166–74.
[55] Barea EM, Gónzalez-Pedro V, Ripollés-Sanchis T, Wu HP, Li LL, Yeh CY, et al. Porphyrin dyes with high injection and low recombination for highly efficient mesoscopic dye-sensitized solar cells. J Phys Chem C 2011;115:10898–902.
[56] Mathew S, Iijima H, Toude Y, Umeyama T, Matano Y, Ito S, et al. Optical, electrochemical, and photovoltaic effects of an electron-withdrawing tetrafluorophenylene bridge in a push–pull porphyrin sensitizer used for dye-sensitized solar cells. J Phys Chem C 2011;115:14415–24.
[57] Teng C, Yang X, Yuan C, Li C, Chen R, Tian H, et al. Two novel carbazole dyes for dye-sensitized solar cells with open-circuit voltages up to 1 V based on Br^-/Br^{3-} electrolytes. Org Lett 2009;23:5542–5.
[58] Ishow E, Brosseau A, Clavier G, Nakatani K, Tauc P, Fiorini-Debuisschert C, et al. Multicolor emission of small molecule-based amorphous thin films and nanoparticles with a single excitation wavelength. Chem Mater 2008;20:6597–9.